Simplified seismic life cycle cost estimation of a steel jacket offshore platform structure

Mohamed Nour El-Din & Jinkoo Kim

Taylor & Francis
Taylor & Francis Group

Simplified seismic life cycle cost estimation of a steel jacket offshore platform structure

Mohamed Nour El-Din and Jinkoo Kim

Department of Civil and Architectural Engineering, Sungkyunkwan University, Suwon, Korea

ABSTRACT

The purpose of the present paper is to develop a simple methodology for seismic life cycle cost (LCC) estimation for a steel jacket offshore platform structure. This methodology accounts for accuracy of LCC modelling as well as simplicity of application. Accuracy is maintained through incorporating the effect of aleatory and epistemic uncertainties in the LCC estimation framework. Simplicity is achieved by using equivalent single-degree-of-freedom (ESDOF) system instead of the full structure and by eliminating full incremental dynamic analysis and fragility analysis. Instead, an approximate fragility curve and a localised incremental dynamic analysis curve are used along with a probabilistic simple closed-form solution for loss estimation. In the design of model structures, different bracing systems are used for the seismic design of the offshore platform, such as conventional and buckling-restrained braces. The proposed LCC methodology is validated through comparison with the results from a more rigorous method. It is found that even though the proposed methodology results in a slightly different solution compared to the reference method, the method can be used as an efficient tool for preliminary LCC evaluation of structures.

1. Introduction

After the large economic losses caused by Northridge Earthquake in 1994, the necessity of the risk-based design approach has been emphasised (Ellingwood & Wen, 2005). However, there are many challenges involved in the quantitative procedures such as the lack of a reliable tool for economic loss quantification, the uncertainty inherited in seismic demand and structural capacity, and the wide range of structural limit states to be considered.

Life cycle cost (LCC) analysis is considered as one of the effective tools for quantitative risk analysis procedures since it explicitly considers the consequences of earthquake events in terms of seismic loss cost. The cost-effective performance of structures under natural hazards such as earthquakes and hurricanes has long been recognised to be an important topic in the design of civil engineering systems (Taflanidis & Beck, 2009). Concerns related to the importance of including LCC in design codes have attracted attention of design profession whether for the conventional design procedures (Wen & Foutch, 1997), or for performance-based design (Hiraishi, Midorikawa, Teshigawara, & Gojo, 1998). From the decision-makers' standpoint, life cycle cost–benefit assessments of seismic risk mitigation activities provide important source of decision supporting information (Goda, Lee, & Hong, 2010). In addition, the LCC assessment is valuable for the consequence-based earthquake engineering (Ellingwood & Wen, 2005).

Generally, researches on the optimal design of offshore structures considering minimum expected LCC, based on the structural initial cost, repair cost and damage cost are relatively rare. One of the early studies on LCC of offshore structures was conducted by Bea, Brandtzaeg, and Craig (1998). In this study, he considered natural and artificial factors to generalise the life cycle risk characteristics of offshore structures using reliability and risk assessment. Garbatov and Soares (2001) used reliability criterion based on the variation in inspection quality to minimise the maintenance costs and highlighted the need for inspections of fatigue failures of floating structures during their lifetime. Ang and Lee (2001) and Ang and Leon (1997) used deformation and energy as damage index for establishing cost functions and applied it to optimum design and reinforced maintenance for offshore structures constructed in Mexico Bay.

De Leon and Ang (2002) formulated cost function of the offshore structure (including repair, injury, fatality and indirect loss cost) based on the damage level. In addition, they proposed a reliability-based cost–benefit optimal decision model for the risk management of oil platforms life cycle considering the integration of socio-economic aspects into the management decision process. Pinna, Ronalds, and Andrich (2003) used cost-effective criteria to investigate the optimum design of monopod platforms considering the economic consequences of failure and the proportion of the fixed cost associated with the construction of the platform. Val and Stewart (2003) calculated LCC for reinforced concrete structures in marine environments under different exposure conditions based on prediction of the expected costs of repair and replacement using a time-variant probabilistic

CONTACT Jinkoo Kim ✉ jkim12@skku.edu

model. Zhang, Li, and Yue (2005) provided an important study on state of the art of structural optimisation for offshore platforms. Li, Zhang, and Yue (2009) proposed an optimum design model of the expected LCC for ice-resistant platforms-based cost-effectiveness criterion. Multiple performance demands of the structure, failure assessment criteria and structural failure mode were considered.

Although significant progress has been made in the last two decades, especially in the field of minimum LCC studies for seismic-designed structures, there have been many uncovered issues found in these studies. Among these issues are: the inadequacy of incorporating the uncertainty in seismic demand and structural capacity, inaccurate modelling of soil-structure interaction, rare investigations of non-building structures, lack of studies on performance-based design approach and the scarcity of studies on the simplified LCC estimation methods for practical use.

The objective of the current study is to develop a seismic LCC methodology that can be easily adapted to seismic applications such as sensitivity or optimisation studies for structures in general with particular emphasis on offshore structures. The methodology accounts for the aleatory and epistemic uncertainties found in LCC components such as seismic fragility and seismic hazard modelling while it maintains the required accuracy with less computational effort. The proposed methodology practically eliminates the need for full incremental dynamic analysis (IDA) or full fragility curves. Instead, the methodology uses an approximate fragility curve (AFC) and localised-incremental dynamic analysis (LIDA). For further simplification, an equivalent-single-degree-of-freedom (ESDOF) system is utilised instead of the full multi-degree-of-freedom (MDOF) model. For verification, the proposed methodology is applied to an offshore platform located in the Gulf of Moattama, which is offshore Myanmar, considering soil–pile structure interaction effect. Also, to investigate the effect of the different seismic design methods on LCC methodology, pile-founded jacket offshore structures with buckling-restrained braces (BRB) and conventional braces are designed using the strength-based design (code procedure) method. The difference in analysis results between the proposed method and similar conventional methods is discussed along with the limitations of the proposed method.

2. Procedure of the simplified LCC method

In this section, a simplified methodology for LCC estimation is presented and suggestions are made for its implementation in practical applications. In the following sections, the elements of the proposed methodology are discussed in details.

2.1. Construction of seismic hazard curve

To obtain earthquake hazard for a given location, several approaches are available, e.g. probabilistic zone maps as used by FEMA P-750 (2009). In the proposed methodology, the dispersion in earthquake demand due to variability in ground motions is established using at least three sets of earthquake ground motions each representing a different hazard level at return periods such as 200, 1000 and 2475 years. Each set includes at least 10 ground motions, which can be selected from any available seismic hazard database, e.g. the PEER database (2013), to represent the hazard at the selected site. In records selection, the following information is considered: the soil type, shear wave velocity, magnitude, fault type and the different distance measures from the site to the fault rupture.

A variety of scaling methods have been used to achieve the correspondence between the hazard levels and the selected ground motion records. Among these methods are amplitude scaling, linear scaling for spectral acceleration at fundamental period of structure (Shome, Cornell, Bazzurro, & Carballo, 1998), linear scaling of spectral acceleration over a period range (Hancock, Bommer, & Stafford, 2008) and linear scaling using spectrum matching (Hancock et al., 2006). Luco and Bazzurro (2007) showed that large scaling factors could introduce a systematic bias to the median nonlinear structural response that tends to increase with decreasing strength and structural period. Iervolino and Cornell (2005) stated that scaling factors up to four do not introduce significant bias to the nonlinear peak displacements of moderate to short period SDOF systems. In the current study, spectrum matching is used to make the geometric mean of the acceleration response spectra of the records compatible with each hazard level selected around the fundamental period of the structure. The scaling factors in the range of 1–4 are used to preserve the fundamental seismological features of the records after scaling.

In the next step, the relation between the elastic spectral acceleration and the hazard function is plotted. Recent comprehensive probabilistic methodologies, such as the Pacific Earthquake Engineering Research center approach (PEER, 2013), use a series of intensity-based loss assessments such that the number of intensities covers (reasonably) the entire hazard curve for the site to calculate expected annual loss of a structure. Typically, a hazard curve will relate the Mean Annual Frequency (MAF), λ, with a relevant Intensity Measure (IM) (e.g. peak ground acceleration, spectral acceleration at the fundamental period, etc.). Assuming that the occurrence of significant earthquakes can be described by a Poisson process, the probability that the ground motion intensity will exceed S_a is modelled by means of the following expression (Kramer, 1996):

$$H\left(S_a\right) = 1 - e^{-\lambda(S_a)t} \tag{1a}$$

where $\lambda(S_a)$ is the average rate of the earthquake occurrence and t is limit period of interest. If the hazard is assumed linear in log–log coordinates, this relation can be approximated by the following form (Cornell, Jalayer, Hamburger, & Foutch, 2002):

$$H\left(s_a\right) = P\left[S_a \geq s_a\right] = k_o s_a^{-k} \tag{1b}$$

where s_a is the elastic spectral acceleration (measure of ground motion intensity); $H\left(s_a\right)$ is the hazard function of spectral acceleration which is the annual probability that the seismic intensity at a site will exceed s_a; k_o and k are the coefficients for linear regression of hazard $H\left(s_a\right)$ on intensity S_a in proximity of limit state probability (region of interest) in logarithmic space. The coefficients k_o and k control the slope and the degree of non-linearity, respectively, of the hazard curve (Aslani & Miranda, 2005). Typical values of the log–log slope k are between one and four (Yun & Foutch, 2000). It tends to be larger (steeper) for high seismic zones such as western U.S. sites and for shorter periods (Cornell et al., 2002).

2.2. Transformation to ESDOF system

In order to maintain simplicity of the methodology, the MDOF system of the original structure is transformed into ESDOF system. The steps involved in the transformation are stated below. The details of this transformation can be found elsewhere (Qi & Moehle, 1991). It is assumed that the response of the structure is dominated by the fundamental vibration mode. Previous studies on fixed type offshore platforms, e.g. Golafshani, Tabeshpour, and Komachi (2009), used the concept of equivalent SDOF system assuming that the structural behaviour is dominated by the first mode. In practice, first mode (sway modes in *x* or *y* direction) is considered to be dominant for the global structural behaviour, and higher modes are commonly considered to be related to local vibration modes like bracing vibrations (Abdel Raheem, 2013). Pushover analysis is used to obtain the structure capacity curve. The lateral force pattern used is in proportion to the product of masses and fundamental mode shape. The capacity curve is transformed to the force–displacement relationship of the ESDOF system. The displacement (u^*) and base shear (V^*) of the ESDOF system are obtained as follows:

$$u* = \frac{\{\Phi\}^T \mathbf{M}\{\Phi\}}{\{\Phi\}^T \mathbf{M}\{1\}}\Delta \tag{2}$$

$$V* = \frac{\{\Phi\}^T \mathbf{M}\{\Phi\}}{\{\Phi\}^T \mathbf{M}\{1\}}V \tag{3}$$

where Φ is the fundamental mode shape vector of the MDOF system; $\mathbf{M}$ is the mass matrix of the MDOF system; $\{1\}$ is the unity vector; Δ and V are the top displacement and base shear of the MDOF system, respectively. The structure capacity curve is idealised as the bilinear force–displacement relationship shown below. Engineering judgement is used to establish this idealised curve, where the area under the idealised and capacity curves should be equal. The guidelines for capacity curve idealisation can be found elsewhere (Fajfar, 2002).

The maximum inter-story drift (MIDR) of the MDOF system can be obtained using the maximum response of the ESDOF system as follows:

$$\text{MIDR(MDOF)} = \text{Max}\left[\left(\Gamma \cdot u_{\text{max}}^*\right) \cdot \frac{\left(\varphi_i - \varphi_{(i-1)}\right)}{h_i}\right] \tag{4}$$

where u_{max}^* is the maximum displacement of the ESDOF; φ_i and $\varphi_{(i-1)}$ are the amplitude of the normalised mode shape at level i and $i-1$, respectively; h_i is the story height between story i and $i-1$; and Γ is the modal participation factor defined as follows:

$$\Gamma = \frac{\{\Phi\}^T \mathbf{M}\{1\}}{\{\Phi\}^T \mathbf{M}\{\Phi\}} \tag{5}$$

In order to quantify the uncertainty of the response estimation using the ESDOF system, probabilistic relationships between analysis results of the ESDOF and the MDOF systems need to be investigated. Jeong and Elnashai (2007) carried out a comparison study of different structural systems such as bridges and building structures to relate the maximum responses of the ESDOF systems to the MDOF systems. It was found that the mean maximum inter-story drift ratio (MIDR) of the MDOF system was equal to the maximum response of the ESDOF system multiplied by 1.07 in case of bridges and 1.13 in case of buildings. Based on their research, the following relationship is used for obtaining mean responses of the offshore platform analysis model structure:

$$\bar{D}_{\text{max}}^{\text{MDOF}} = 1.1\,\bar{D}_{\text{max}}^{\text{ESDOF}} \tag{6}$$

where $\bar{D}_{\text{max}}^{\text{MDOF}}$ and $\bar{D}_{\text{max}}^{\text{ESDOF}}$ are the mean maximum demand of the MDOF and ESDOF systems, respectively.

2.3. Hazard selection check using fragility function

The criterion for record selection is based on the probability of exceedance of a specific limit state achieved using the record set with a certain return period (e.g. 200 yr). This probability of exceedance can be obtained using suitable fragility function. For example, for the 10 records of the 200 yr hazard, first nonlinear time history analyses (NLTHA) are conducted on the ESDOF, then the median and the standard deviation of the MIDR are obtained. The probability of MIDR to reach or exceed a specific limit state (LS) at a given earthquake intensity (s_a) is obtained as follows (Aslani & Miranda, 2005):

$$P(\text{LS}_{|s_a}) = \Phi\left[\frac{\ln\text{MIDR}_{\text{LS}} - \ln(\lambda_D)}{\tilde{\sigma}_D}\right] \tag{7}$$

in which Φ is the cumulative normal distribution function, $\tilde{\sigma}_D$ is the logarithmic standard deviation of the MIDR evaluated at a given intensity measure S_a. Parameter $\tilde{\sigma}_D$ can be estimated as the sample counted median or as the harmonic mean of the sample.

In the proposed method, the variation of the median structural response with changes in ground motion intensity is given by (Aslani & Miranda, 2005):

$$\lambda_D = \alpha_1.\alpha_2^{S_a}.(S_a)^{\alpha_3} \tag{8}$$

where S_a is the ground motion intensity measure, and parameters α_1, α_2 and α_3 are constants that are computed from a regression analysis with the three known ($S_a - \lambda_D$) pairs. The function to represent changes in logarithmic standard deviation of structural response parameters with changes in ground motion intensity is given by (Aslani & Miranda, 2005):

$$\tilde{\sigma}_D = \beta_1 + \beta_2 \cdot S_a + \beta_3(S_a)^2 \tag{9}$$

where parameters β_1, β_2 and β_3 are constants that are computed from a regression analysis with the three known ($S_a - \lambda_D$) pairs.

It is worth mentioning that there is no need to construct the whole fragility curve in this stage, since only one point on the fragility curve is required for each specific hazard record. These points will be used later for the construction of what will be called the AFC. In order to obtain the AFC, it is required to maintain $P(\text{LS}_{|s_a})$, the probability of exceeding certain limit state, to be around 50%. This is important to make straight line fitting with constant slope around the $P(\text{LS}_{|s_a}) = 50\%$. If $P(\text{LS}_{|s_a})$ values are too small or too large (i.e. far from $P(\text{LS}_{|s_a}) = 50\%$), then other

hazard records should be selected for the same structure site location to obtain reasonable probability values not far from 50%.

2.4. Relation of demand and hazard intensity

The relationship between drift demand (D) and hazard intensity (S_a) can be accurately described through nonlinear dynamic-response time history analysis (NLTHA) which is the basis of the method proposed in this study. To this end, a regression analysis of the structure responses as a function of the excitation intensity measure is performed. In view of the nonlinear nature of the problem and large scatter of the response due to record-to-record variation, a nonlinear regression analysis of the power-law form (Luco & Cornell, 2001) is used since it is simple and flexible:

$$\widehat{D} = a(S_a)^b \qquad (10)$$

where $\widehat{D}$ is the median drift demand; S_a is the elastic spectral acceleration (measure of ground motion intensity); a and b are the regression coefficients for linear regression of drift demand D at intensity S_a in logarithmic space. Alternatively, the following equation can be used as described in the previous section (Aslani, 2005):

$$\widehat{D} = \alpha_1 \cdot \alpha_2^{S_a} \cdot (S_a)^{\alpha_3} \qquad (11)$$

where α_1, α_2 and α_3 are constants determined by curve fitting to the data points that match the spectral acceleration at the fundamental period with the median drift of the earthquake demand.

The most practical way to estimate the regression parameters, a and b, is to perform nonlinear dynamic time history response analysis (NLTHA) on the ESDOF system using all records with scaling each record set to the corresponding intensity measure at the fundamental period of the structure. One can plot the relation between the drift-demand and the intensity, and then conduct a regression analysis of ($\ln D$) on ($\ln S_a$). A simpler option, with less accuracy, may be applied in which the median ground motion for each set of records is used for the NLTHA instead of using all records. This median ground motion needs engineering judgement to be selected and shall be representative of the whole records set.

2.5. Estimation of median drift capacity intensity using AFC

The median drift capacity intensity, $S_a^{\hat{c}}$, is the intensity measure that corresponds to the probability of exceedance equal to 50% of a specific limit state. In this step, $S_a^{\hat{c}}$ is estimated using the AFC. After construction of the relation between the median drift and the hazard intensity, the drift data, i.e. the maximum drifts corresponding to all records, are used to construct an AFC for a given limit state. In this study, the performance levels such as immediate occupancy (IO), life safety (LS) and collapse prevention (CP) are used as limit states as defined in FEMA 356 (2000). This curve can be constructed after having the median and standard deviation of drift for all responses obtained from NLTHA as explained in the previous step.

For explanation purposes, let us assume that for a specific limit state, the corresponding probabilities $P(\text{LS}_{|s_a})$ calculated
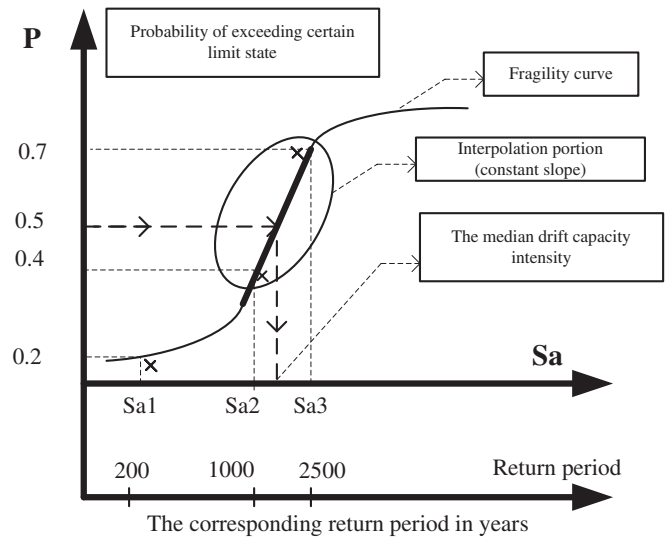

Figure 1. Sketch for extracting the median capacity intensity using the approximate fragility curve (AFC).

for the 200, 1000 and 2500 yr hazards are, .2, .4 and .7, respectively. Using these values, one can plot the relation between the intensity measure and the probability of exceedance as shown in Figure 1. One can draw the AFC by three points only (S_a, $P(\text{LS}_{|s_a})$), as discussed in the construction of AFC in the previous steps. Assumption is made that the slope of fragility curve is constant around $P(\text{LS}_{|s_a}) = 50\%$. Then, it is required to make a curve fitting for 2 or 3 points to predict the accurate location of $P(\text{LS}_{|s_a}) = 50\%$ on the plot. From the figure, one can obtain the spectral acceleration corresponding to the median drift capacity (i.e. $S_a^{\hat{c}}$). This spectral acceleration can be found easily by interpolation among the points used for constructing the AFC.

The main differences in the estimation of $S_a^{\hat{c}}$ between FEMA P695 (2009) and the proposed methodology can be summarised as follows: Firstly, in FEMA P695, only building systems are investigated and assumptions are not suitable for non-building structures (such as fixed steel offshore structures). In addition, FEMA P695 method is consistent with the 'life-safety' performance objective only, whereas more than one limit state is required to estimate the seismic LCC of a structure. Secondly, in FEMA P695, the record-to-record collapse uncertainty is set to a fixed value (equals to .4 for systems with period-based ductility equal to or larger than three). However, in the proposed methodology the demand dispersion uncertainty (which includes record-to-record uncertainty) is accurately estimated at each median collapse intensity $S_a^{\hat{c}}$ as will be discussed in the following section. Thirdly, in FEMA P695 IDA is used to obtain $S_a^{\hat{c}}$ by scaling all records to the maximum considered earthquake intensity, and then increasing the intensity until one-half of the scaled ground motion records cause collapse of the system. This may require more NLTHAs compared to the proposed method.

2.6. Estimation of demand dispersion using localised IDA

In this step, NLTHA is performed using the ESDOF system for all records (e.g. 30 records) scaled to the specified $S_a^{\hat{c}}$ to get the dispersion in demand $\beta_{D|s_a}$ for each limit state. LIDA is performed instead of full IDA using records scaled to the specific $S_a^{\hat{c}}$. Based on the
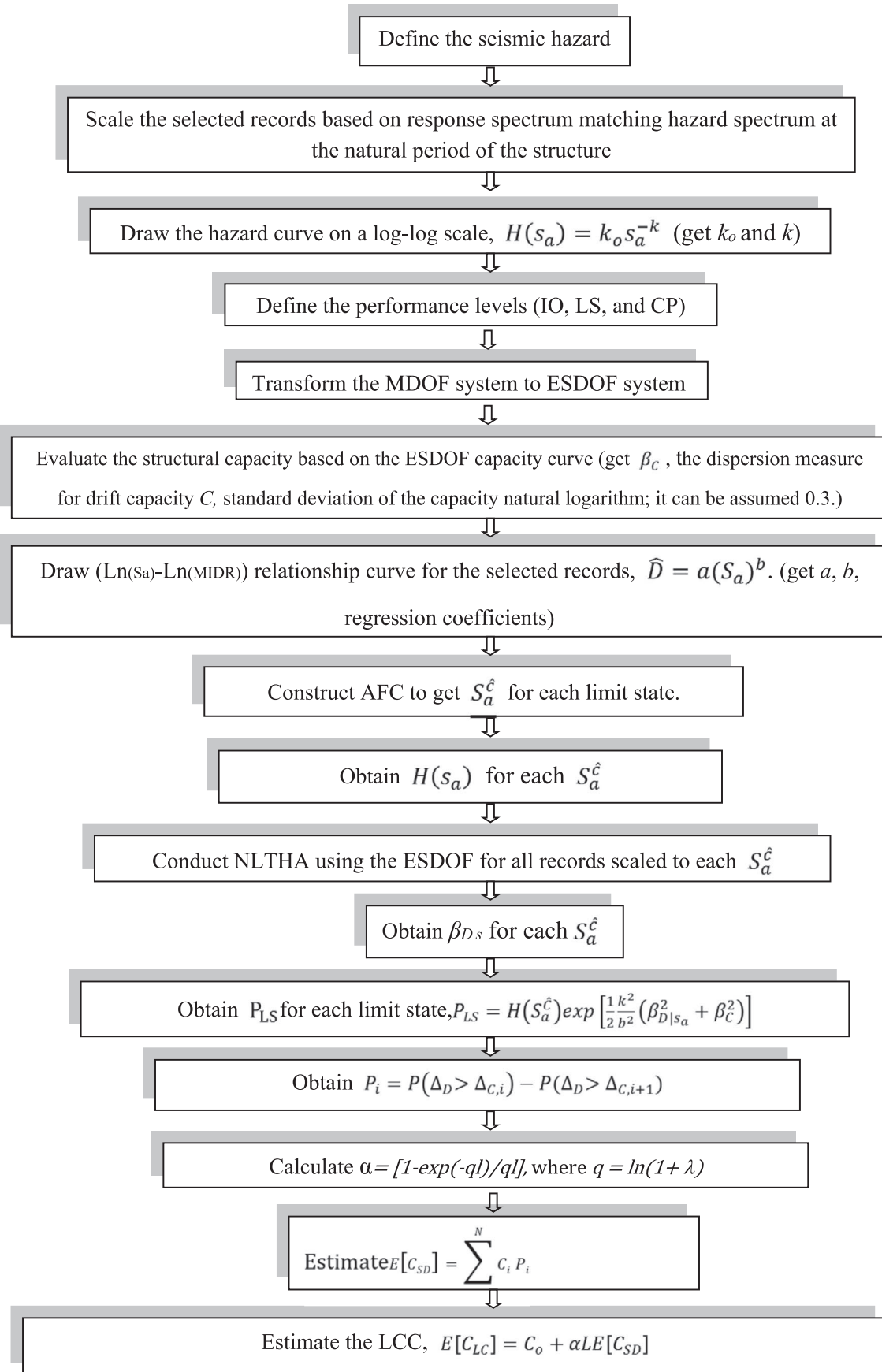
Define the seismic hazard

⇩

Scale the selected records based on response spectrum matching hazard spectrum at the natural period of the structure

⇩

Draw the hazard curve on a log-log scale, $H(s_a) = k_o s_a^{-k}$ (get k_o and k)

⇩

Define the performance levels (IO, LS, and CP)

⇩

Transform the MDOF system to ESDOF system

⇩

Evaluate the structural capacity based on the ESDOF capacity curve (get β_C , the dispersion measure for drift capacity C, standard deviation of the capacity natural logarithm; it can be assumed 0.3.)

⇩

Draw (Ln(Sa)-Ln(MIDR)) relationship curve for the selected records, $\widehat{D} = a(S_a)^b$. (get a, b, regression coefficients)

⇩

Construct AFC to get $S_a^{\hat{c}}$ for each limit state.

⇩

Obtain $H(s_a)$ for each $S_a^{\hat{c}}$

⇩

Conduct NLTHA using the ESDOF for all records scaled to each $S_a^{\hat{c}}$

⇩

Obtain $\beta_{D|s}$ for each $S_a^{\hat{c}}$

⇩

Obtain $\mathrm{P_{LS}}$ for each limit state, $P_{LS} = H(S_a^{\hat{c}})exp\left[\frac{1}{2}\frac{k^2}{b^2}\left(\beta_{D|s_a}^2 + \beta_C^2\right)\right]$

⇩

Obtain $P_i = P(\Delta_D > \Delta_{C,i}) - P(\Delta_D > \Delta_{C,i+1})$

⇩

Calculate α = [1-exp(-ql)/ql], where $q = ln(1+\lambda)$

⇩

Estimate $E[c_{SD}] = \sum_{}^{N} c_i P_i$

⇩

Estimate the LCC, $E[C_{LC}] = C_o + \alpha L E[C_{SD}]$

Figure 2. Sequence of the proposed LCC methodology.
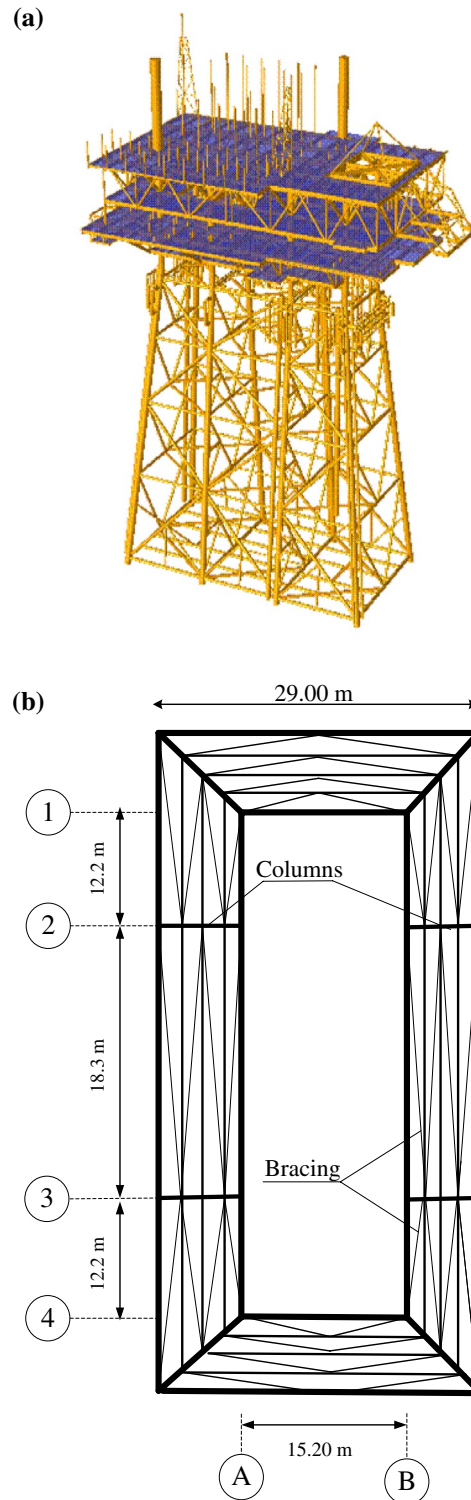
(a)

(b)

Figure 3. Jacket structure schematic views: (a) perspective plot of the actual platform; (b) plan view of the jacket; (c) 2-D single frame extracted from the actual platform with the soil–pile configuration.

MIDR obtained from this NLTHA, the median MIDR (μ) and the standard deviation ($\beta_{D|s_a}$) of MIDR can be obtained, where $\beta_{D|s_a}$ is the dispersion measure for drift demand D at a given S_a level. Then, the median and standard deviation of the MIDR are used to calculate the accurate probability, corresponding to each $S_a^{\hat{c}}$, for each specific limit state. This is to ensure that the corresponding probability of failure is 50%. It will be accepted if the probability falls within the range of 45–55%. Unlike other studies (Sullivan, Welch, & Calvi, 2014), the dispersion in demand $\beta_{D|s_a}$ is not assumed but is estimated accurately for each limit state as discussed above. Even though there are some NLTHAs conducted on the ESDOF, the computational cost is still minimum compared to performing full IDA.
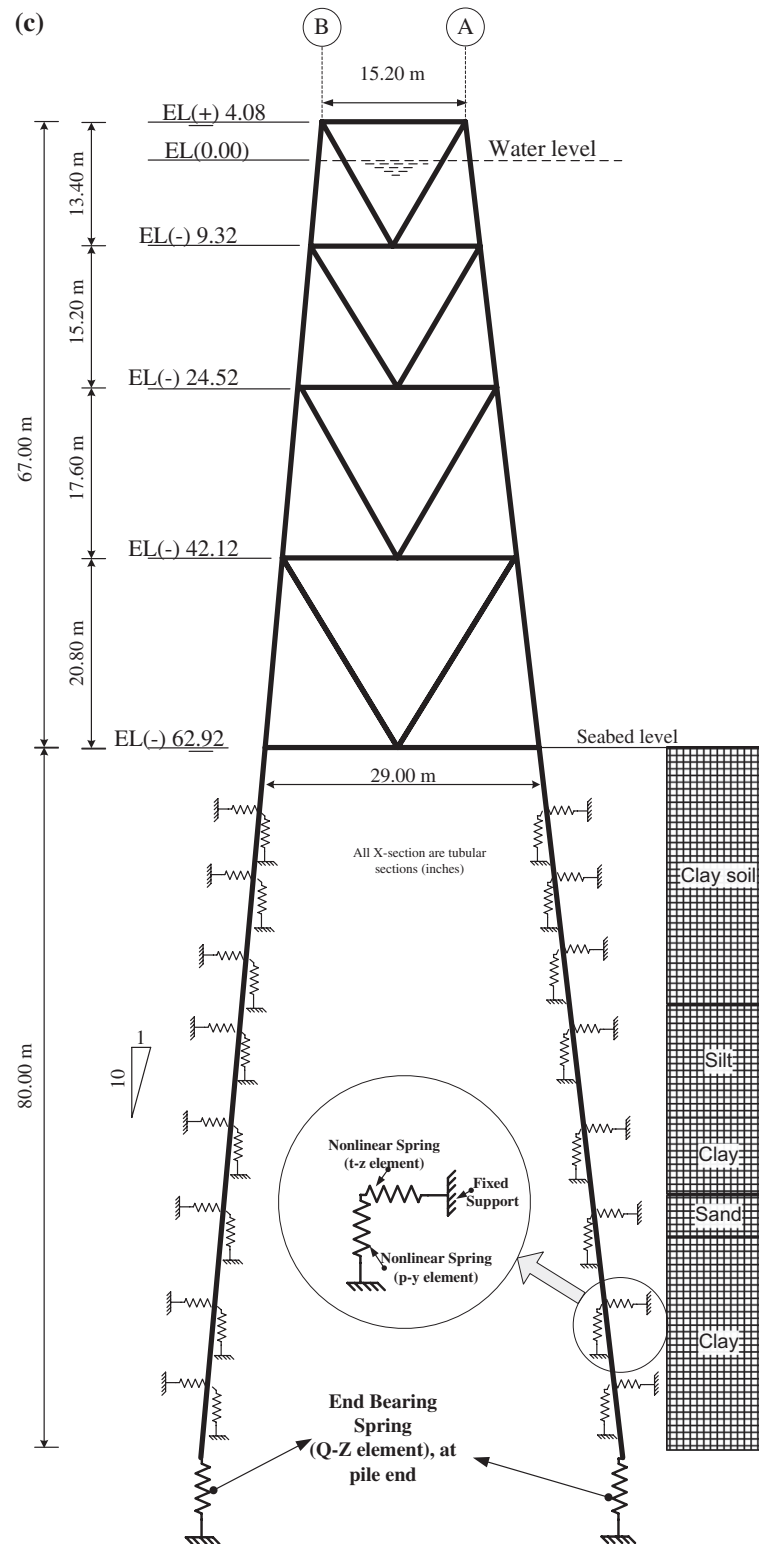
(c)

Figure 3. (*Continued*)

2.7. Damage state probability

The next step in the process of LCC evaluation is the calculation of the damage state probabilities, i.e. the probability of the structure attaining the pre-defined damage states throughout its lifetime. For simplicity, the uncertainties in the seismic hazard, structural demand and structural capacity models are assumed as lognormal variables with a median and standard deviation values. The annual probability of exceeding a selected limit state (LS) can be determined as follows (Pinto, Giannini, & Franchin, 2004):

$$P_{LS} = \int_0^\infty P\left(LS_{S_a=s_a}\right) \left| \frac{dH(s_a)}{ds_a} \right| ds_a \qquad (12)$$

where $P(.)$ is the probability of exceeding the LS limit state if the intensity measure (S_a) is equal to S_a, and $H(S_a)$ is the hazard of the intensity measure. In other words, the first and the second terms in the integral represent the fragility function and the slope of the mean annual rate of exceedance of the ground motion intensity, respectively.

Cornell et al. (2002) have shown that the above equation can be approximated using the following simple closed-form solution:

$$P_{LS} = H\left(S_a^{\hat{C}}\right)\exp\left[\frac{1}{2}\frac{k^2}{b^2}\left(\beta_{D|s_a}^2 + \beta_C^2\right)\right] \quad (13)$$

where P_{LS} is the damage state probability; $S_a^{\hat{C}}$ is the spectral acceleration corresponding to the median drift capacity (obtained from the AFC); $H(.)$ is the seismic hazard function of spectral acceleration which is the annual probability that intensity S_a at a site will equal or exceed s_a (obtained from Equation (1)); k is one of the coefficients for linear regression of hazard $H(S_a)$ on intensity S_a in proximity of limit state probability in logarithmic space, which controls the degree of nonlinearity of the hazard curve (can be obtained from fitting the hazard curve or from Equation (1b)); b is one of the regression coefficients for linear regression of drift demand D on intensity S_a in logarithmic space (section 2.6); $\beta_{D|s}$ is the dispersion measure for drift demand D at given S_a level (obtained from the LIDA at the specified S_a); and β_C is dispersion measure for drift capacity C (standard deviation of natural logarithm), which is assumed to be .3 based on previous studies (Cornell et al., 2002). In the above equation, the effects of randomness and uncertainty are combined. Note that the expected damage state probability is equal to the mean estimate value of the hazard exceeding the median structural capacity multiplied by a correction factor. This factor increases exponentially with the total uncertainty in the demand and capacity, and depends on the hazard and regression analysis parameters (k and b).

2.8. LCC formulation

Once the damage state probabilities are calculated, the expected LCC of a structure can be calculated as (Wen & Kang, 2001):

$$E[C_{LC}] = C_o + \int_0^L E[C_{SD}]\left(\frac{1}{1+\lambda}\right)^t dt = C_o + \alpha L E[C_{SD}] \quad (14)$$

where C_o is the initial construction cost which will be related to the material cost in the current study, L is the service life of the structure, λ is the annual discount rate and $E[C_{SD}]$ is the annual expected seismic damage cost which is governed by a Poisson process (implicit in hazard modelling) and does not depend on time. It is assumed that structural capacity does not degrade over time and the structure is restored to its original condition after each hazard. On the right-hand side, α is the discount factor which is equal to $[1 - \exp(-ql)/ql]$, where $q = \ln(1+\lambda)$. Hence, $E[C_{SD}]$ is given by:

$$E[C_{SD}] = \sum_{i=1}^{N} C_i P_i \quad (15)$$

Table 1. Details of the tubular sections and BRBs used in the model structures.

Members	Story	FB-BRB (cm²)	FB-Conv (cm)
Braces	1		
		50.9	55×2.5
	2	50.9	60×2.2
	3	46.3	50×2.6
	4	40.7	50×2.2
Columns	1	95×5.0	110×5.0
	2	95×4.0	100×4.5
	3	80×3.8	90×4.0
	4	75×3.2	90×4.0
Beams	1	75×4.6	75×4.5
	2	75×3.6	80×4.2
	3	70×3.4	75×4.0
	4	55×2.75	50×2.5

Table 2. Design parameters for model structures FB-BRB and FB-Conv models.

S_{DS} (g)	1.0
S_{D1} (g)	.7
Framing type	BRBF (FB-BRB)
	OCBF (FB-Conv)
Response Modification Factor, R	7 (FB-BRB)
	3.25 (FB-Conv)
Importance factor, I	1
Occupancy category	II
Seismic design category	D
Base shear coefficient (Base shear/structure weight)	.052 (FB-BRB)
	Base shear = 1941 kN
	.11 (FB-Conv)
	Base shear = 4107 kN
Fundamental period (sec)	2.75 (FB-BRB)
	1.8 (FB-Conv)

Table 3. Dynamic characteristics of the structural models.

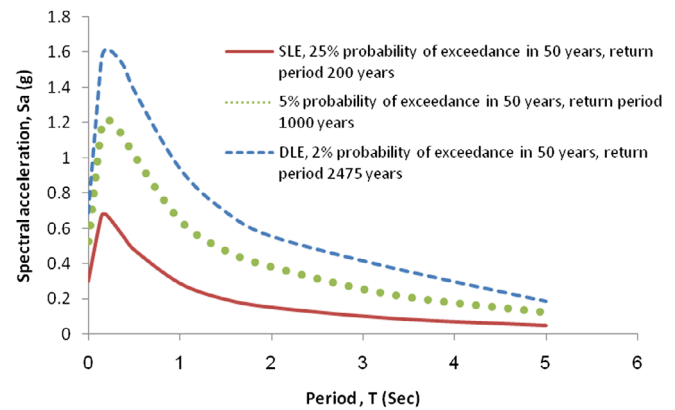|	FB-BRB			FB-Conv		
Mode	1	2	3	1	2	3
Natural periods (sec)	2.75	.86	.47	1.8	.45	.4
Mass participation factor	.83	.06	.01	.8	.09	0

Figure 4. Design spectra at different return periods obtained at gulf of Mottama, offshore Myanmar.

where N is the total number of limit-states considered, P_i is the total probability that the structure is in the ith damage state throughout its lifetime and C_i is the corresponding cost.

In accordance with the definition of seismic hazard, three structural damage states are used (i.e. N is equal to three) such as IO, LS and CP, and C_i is assumed to be 30, 70 and 100%,

Table 4. Characteristics of the ground motion suit used in the NLTH analysis.

	No.	NGA#[a]	Event	Station	Mag.	R_{jb}[b] (km)	R_{rup}[c] (km)
DLE	1	832[d]	Landers	Amboy	7.28	69.2	69.2
	2	860	Landers	Hemet Fire Station	7.28	68.7	68.7
	3	886	Landers	Puerta La Cruz	7.28	94.5	94.5
	4	888[d]	Landers	San Bernardino – E & Hospitality	7.28	79.8	79.8
	5	891	Landers	Silent Valley – Poppet Flat	7.28	50.9	50.9
	6	1147[d]	Kocaeli – Turkey	Ambarli	7.51	68.1	69.6
	7	1149	Kocaeli – Turkey	Atakoy	7.51	56.5	58.3
	8	1154	Kocaeli – Turkey	Bursa Sivil	7.51	65.5	65.5
	9	1155[d]	Kocaeli – Turkey	Bursa Tofas	7.51	60.4	60.4
	10	1163	Kocaeli – Turkey	HavaAlani	7.51	58.3	60.0
SLE	11	1627	Caldiran – Turkey	Maku	7.21	50.8	50.8
	12	1637	Manjil – Iran	Rudsar	7.37	64	64.5
	13	1640	Manjil – Iran	Tonekabun	7.37	93.3	93.6
	14	1766	Hector Mine	Baker Fire Station	7.13	64.1	64.8
	15	1767	Hector Mine	Banning – Twin Pines Road	7.13	83.4	83.4
	16	1773	Hector Mine	Cabazon	7.13	76.9	76.9
	17	1776	Hector Mine	Desert Hot Springs	7.13	56.4	56.4
	18	1782	Hector Mine	Forest Falls Post Office	7.13	74.9	74.9
	19	1783	Hector Mine	Fort Irwin	7.13	65	65.9
	20	1786	Hector Mine	Heart Bar State Park	7.13	61.2	61.2

[a]Next Generation of Ground-Motion Attenuation Models;
[b]Joyner–Boore distance (km): the horizontal distance to the surface projection of the rupture plane;
[c]closest distance (km) to the fault rupture plane;
[d]used for DLE (ductility level earthquake) design.
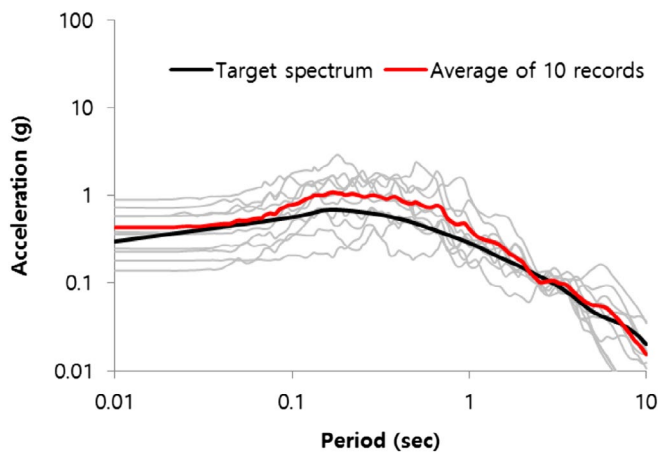
(a) Strength-level earthquake
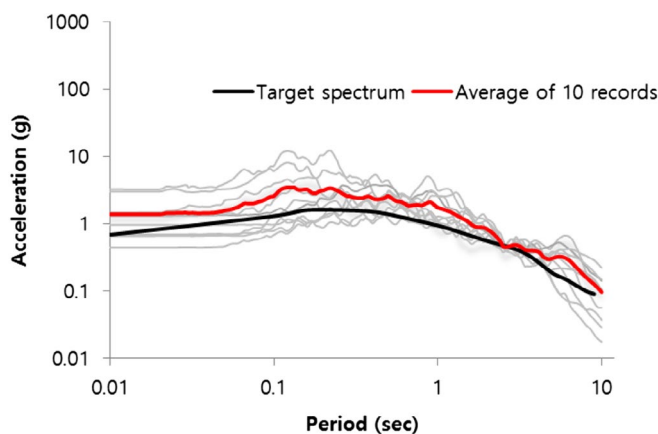
(b) Ductility-level earthquake

Figure 5. Response spectra of the ground motions and their geometric mean with the target spectra for two-level earthquakes: (a) 2% and (b) 25% probability of exceedance in 50 years.

respectively, of the initial cost of the structure. This is based on the correspondence of these damage states with the information provided by Fragiadakis, Lagaros, and Papadrakakis (2006) and P_i is given by:

$$P_i = P\left(\Delta_D > \Delta_{C,i}\right) - P(\Delta_D > \Delta_{C,i+1}) \qquad (17)$$

where Δ_D is the earthquake demand and $\Delta_{C,i}$ is the structural capacity, usually represented in terms of drift ratio, defining the ith damage state. The probability of demand being greater than capacity $\delta_D > \delta_{C,i}$ is evaluated as discussed in the previous step. The sequence of the proposed LCC methodology is given in Figure 2.

2.9. Characteristics of the proposed methodology

Even though seismic LCC evaluation provides deeper insight into the seismic performance of a structure and the effectiveness of a seismic retrofit method, it is rarely applied in practice, mainly due to the huge computational demands involved in the statistical evaluation of a nonlinear system. In the proposed method, an ESDOF system is used instead of full model generally used in similar studies (Gencturk, 2013) to reduce the computation time required for NLTH analyses. In order to obtain and quantify the dispersion of the seismic demand, a localised IDA is used instead of full IDA as done by Dolsek (2012) and Fragiadakis and Vamvatsikos (2010). In addition, AFCs are used instead of the full curves to obtain the spectral acceleration at the drift capacity ($S_a^{\hat{c}}$).

In addition to the simplicity of computation, the method incorporates different types of uncertainties including aleatory and epistemic uncertainties. The uncertainties in demand and capacity are explicitly considered in the loss estimation equation through $\beta_{D|s}$ and β_C. The dispersion in demand ($\beta_{D|s_a}$) is calculated based on NLTHA for all records using ESDOF system and is not based on experience as in Cornel et al. (2002) study or assumed as in Sullivan et al. (2014)
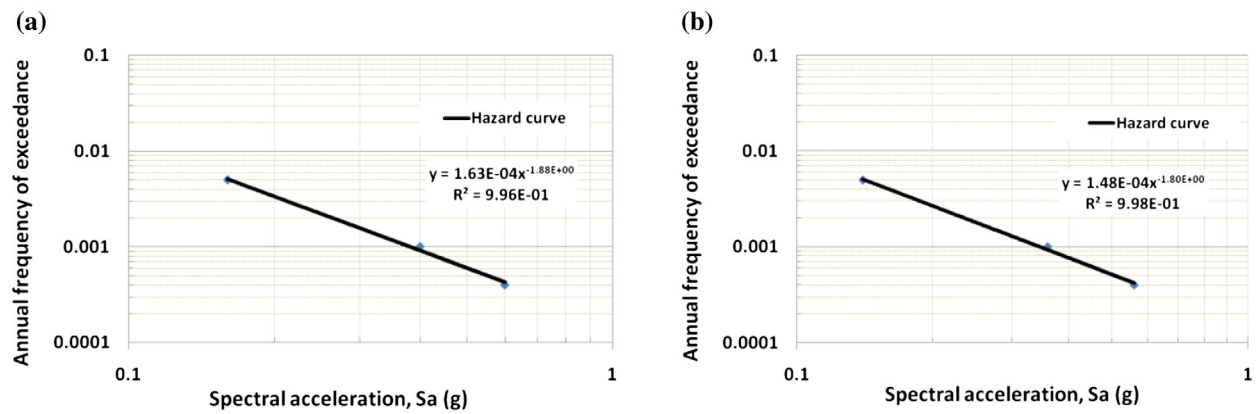
(a)

(b)

Figure 6. Earthquake hazard curve at gulf of Mottama, offshore Myanmar on a logarithmic scale for FB-Conv: (a) MDOF, (b) ESDOF.

(a)

(b)

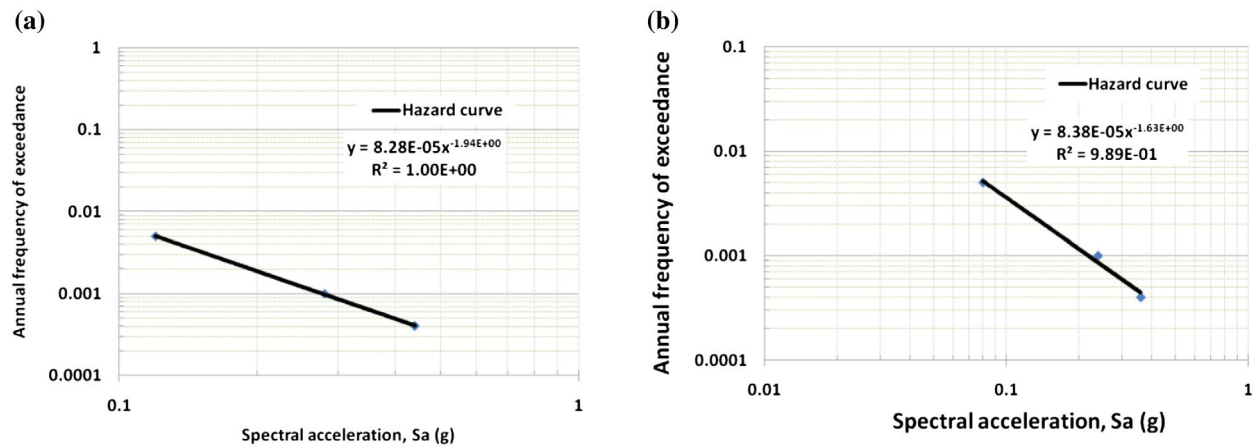**Figure 7.** Earthquake hazard curve at gulf of Mottama, offshore Myanmar on a logarithmic scale for FB-BRB: (a) MDOF, (b) ESDOF.
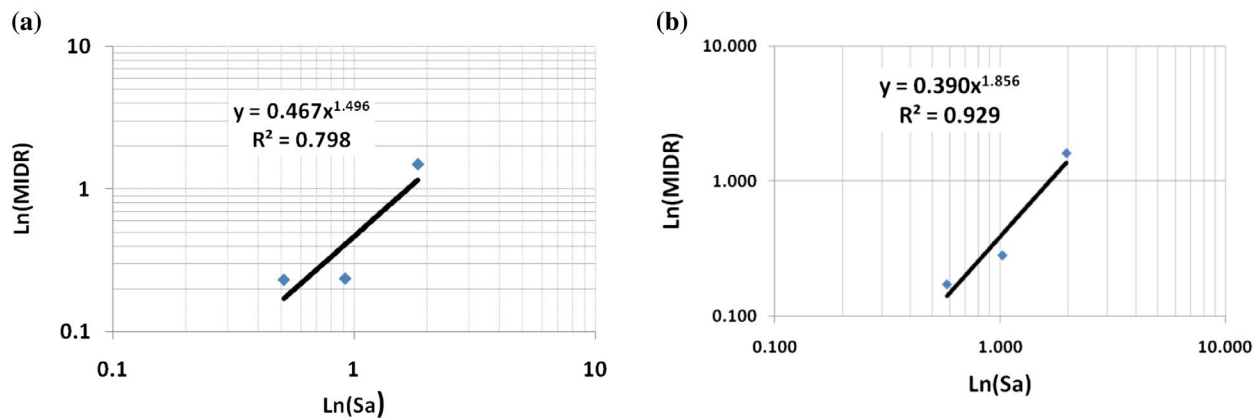
(a)

(b)

Figure 8. Earthquake demand-spectral acceleration curve fitting on a logarithmic scale for FB-Conv: (a) MDOF, (b) ESDOF.

and Welch, Sullivan, and Calvi (2014) studies. The regression coefficients of the demand-intensity relation and the hazard curve, i.e. k and b, are explicitly considered in the loss estimation equation. It also needs to be pointed out that the study is conducted based on the assumption that the structural capacity does not degrade with time and the structure is restored to its original condition after each hazard as done in other similar studies (Gencturk, 2013). In addition, it is assumed that the structural response is dominated by the fundamental mode of vibration.

3. Case study and hazard selection

Most of the simplified methods proposed previously use building structures as case studies (e.g. Sullivan et al., 2014). These methods are primarily based on some assumptions suggested by FEMA guidelines (FEMA P58-1, 2012) for buildings. It is important to mention that such guidelines, which provide simplified tools for construction of fragility curves and assumptions for demand and capacity dispersion, have not been tested on
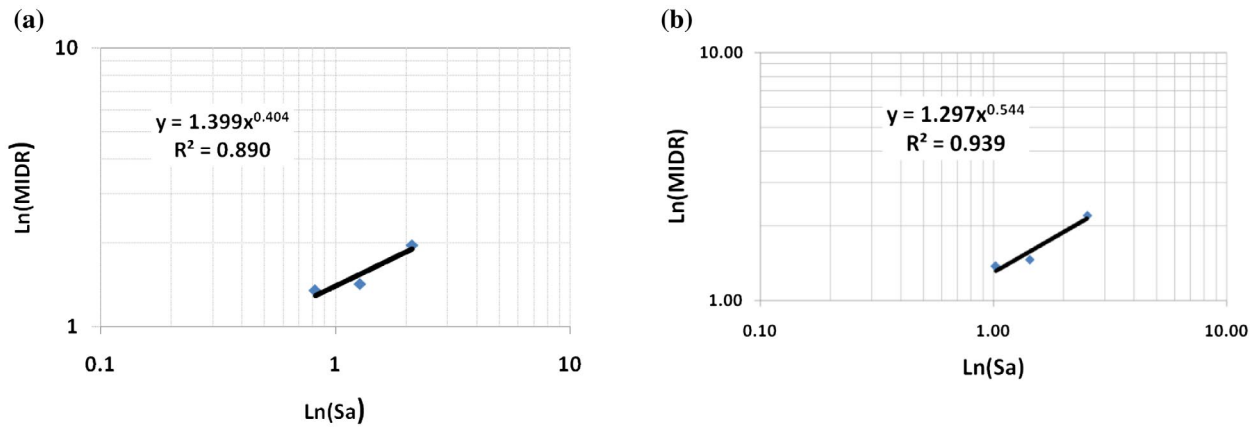
(a)

y = 1.399x^{0.404}
R² = 0.890

(b)

y = 1.297x^{0.544}
R² = 0.939

Figure 9. Earthquake demand-spectral acceleration curve fitting on a logarithmic scale for FB-BRB: (a) MDOF, (b) ESDOF.
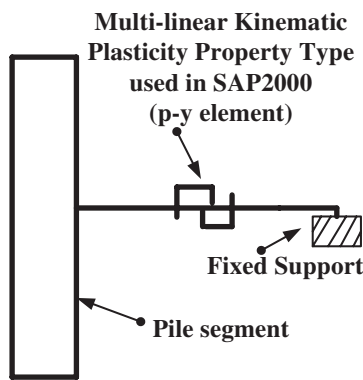

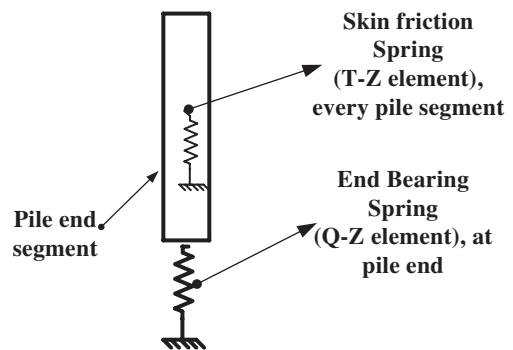**Figure 10.** Configuration of lateral soil stiffness modelled in SAP2000.

Figure 12. Schematic illustration of the pile spring model.

non-building structures. In the current study, the proposed methodology is validated by applying it to a fixed-type steel offshore platform located in Gulf of Moattama, offshore Myanmar, shown in Figure 3.

3.1. Numerical modelling and hazard selection

The numerical modelling of the case-study platform includes full soil–pile-structure interaction (SPSI) modelling. The jacket structures are designed based on the force-based (or code-based) design method (AISC 360-05, 2005). For comparison purposes,

two different circular hollow-section bracing systems are used, the first is a conventional bracing system, FB-Conv; the second is a buckling-restrained bracing system, FB-BRB. The overall configuration and member sizes of the platform case-study structures are also shown in Figure 3 and Table 1, respectively. The design parameters for model structures and the dynamic characteristics of the structural models are given in Tables 2 and 3, respectively. The detailed description of the case-study platform, the design methods used and the earthquake ground motions of the platform site are provided in details elsewhere (Nour El-Din & Kim, 2015).
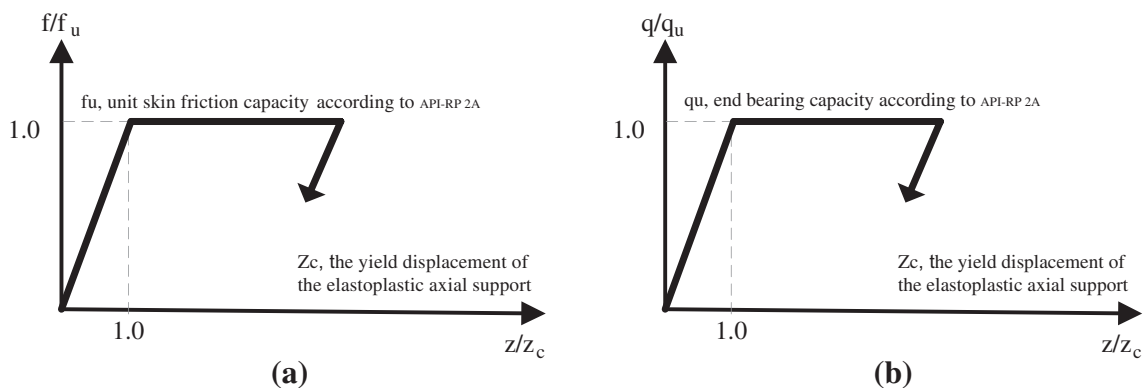

Figure 11. Axial load–deflection curves for clays and sands (Anagnostopoulos, 1983; Coyle & Reece, 1966). (a) Skin friction. (b) End bearing.
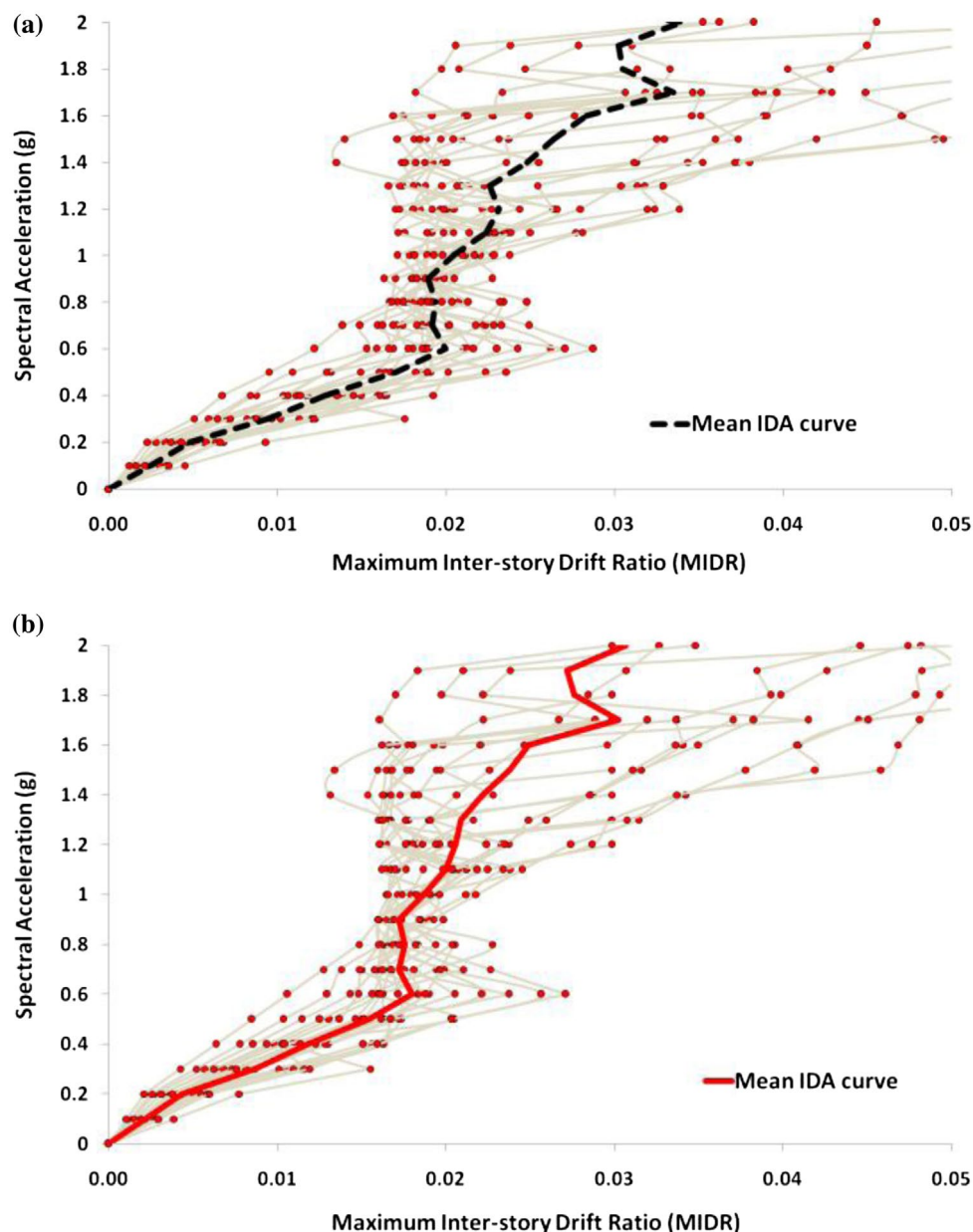
(a)

(b)

Figure 13. IDA curves for FB-Conv model with the mean indicated: (a) MDOF, (b) ESDOF.

In this study, nonlinear analyses are conducted on the representative 2D-frame models. The brace elements are modelled as truss elements and Jacket legs are modelled as frame elements (beam–columns). The jacket horizontal members are frame elements (beams) pin-connected at the ends. A pinned beam–column–brace connection is used at all story levels to avoid undesirable connection failures due to unbalanced brace forces. The model structures are designed with compact sections so that local buckling is prevented. The local behaviours of joints are not considered based on the assumption that they are designed to be stronger than elements using larger safety factor.

The mass used in the dynamic analysis consists of the mass of the platform associated with gravity loading defined, the mass of the fluids enclosed in the structure and the appurtenances, and the added mass. The mass of the model frame is applied at each joint, while the mass from the top side structure is applied at

the upper two joints of the jacket frame. The nonlinear dynamic analyses of the model frame structure are carried out using the SAP2000 software (2005). A frame element with plastic hinges is chosen from the SAP2000 library to model the nonlinear behaviour of platform members. The modal damping ratio of 5% of critical damping is generally used in the analysis of offshore structures (API RP-2A, 2000), which includes the effect of water–structure interaction and the foundation- and structure-related energy dissipation effects.

Figure 4 depicts the design spectra of earthquake loads with three different intensity levels, such as earthquakes with return periods of 200, 1000 and 2475 years. Table 4 shows the characteristics of the ground motion suits representing the strength level earthquakes (SLE) and the ductility level earthquakes (DLE), which are earthquakes with return period of 200 and 2475 years, respectively. Each set includes 10 ground motions
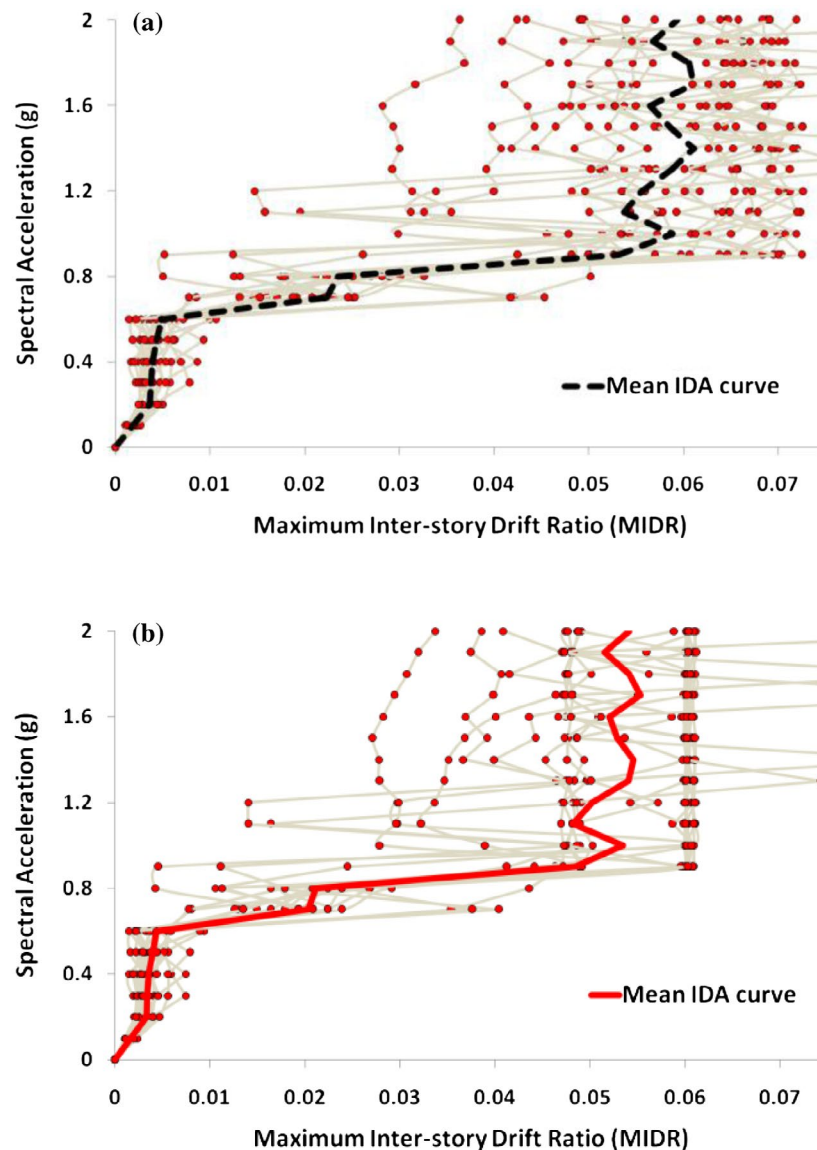
Figure 14. IDA curves for FB-BRB model with the mean indicated: (a) MDOF, (b) ESDOF.

selected from the PEER database (2013) to represent the hazard at the selected site. The spectrum matching method is used to make the geometric mean of the acceleration response spectra of the records compatible with each target hazard level spectrum at the fundamental period of the structure. The scaled record sets used in the current study for both the strength and the DLE with 2% and 25% probability of exceedance in 50 years are given in Figure 5 along with the mean and the target spectra. The hazard curves of the FB-Conv model obtained from Equation (1) for both the MDOF and the ESDOF systems are shown in Figure 6. For FB-BRB, the corresponding hazard curves are shown in Figure 7. Figures 8 and 9 illustrate the demand-seismic hazard relation used in the current study obtained from Equation (11) for FB-Conv and FB-BRB models, respectively.

3.2. SPSI modelling

In the present study, the Beam on Non-Linear Winkler Foundation (BNWF) model is applied to approximate the

interaction between the pile and the surrounding soil (Matlock, 1970), in which parallel nonlinear soil–pile springs are used along the pile penetration length. This model simplifies the interaction between the soil and the pile by assuming that the displacement of one spring has no effect on the displacement of other springs. The lateral soil stiffness is modelled using the p–y approach. In this approach, for each layer of soil along the depth, a nonlinear relationship is established between the lateral pile displacement (y) which mobilises the lateral soil reaction (p) per unit length. The procedure of generating p–y curves is recommended in American Petroleum Institute Standard API RP-2A (2000).

In the present study, p–y curves are based on the actual soil data extracted from the geotechnical report of the platform site (PTTEP International, 2010). In the numerical model proposed in this paper, the Multi-Linear Plastic-type link element in SAP2000 is used to model the nonlinear lateral relation between the soil and the pile. In that link element, the nonlinear link stiffness for the axial degree of freedom is defined according to the
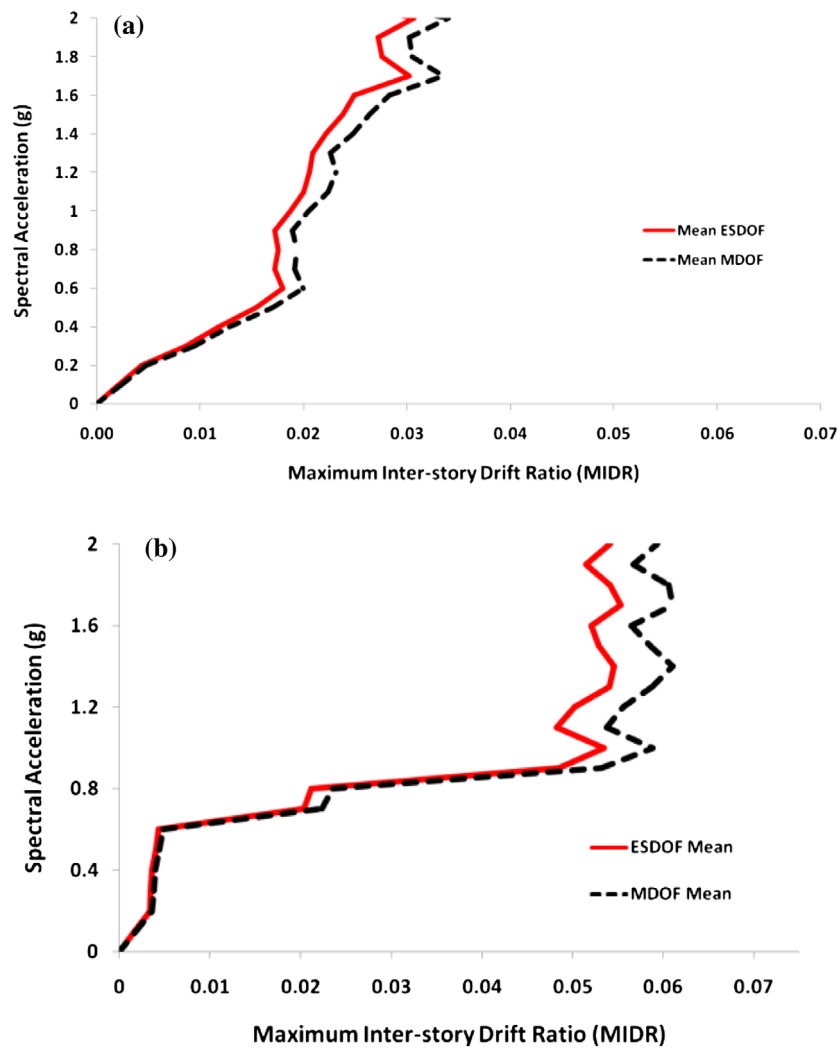
Figure 15. Comparison between the mean IDA curves for both the MDOF and the ESDOF systems: (a) FB-Conv, (b) FB-BRB.

Figure 16. Fragility curves for the FB-Conv model at three limit states obtained from the reference method (Ref) and the approximate method (AFC).

p–y curve. Then, the p–y curve is redefined as a force–deformation (F–D) relationship where F is the total force acting along the

tributary length of a pile joint. After that, a lateral link is defined for each joint along each unit pile segment to represent the lateral

soil nonlinear behaviour. Figure 10 displays the configuration of the proposed model in SAP2000. A multi-linear kinematic plasticity property type is selected for uniaxial deformation from the SAP2000 library to model the hysteresis of the non-gapping soil behaviour.

The skin friction and the end bearing between a pile and the surrounding soil produce the soil resistance to the axial movement of the pile. Each of the resistance action is characterised by a nonlinear force–deformation relationship. Experimental results suggest that these force–deformation characteristics may be adequately represented by the elastic, perfectly plastic relationship (Anagnostopoulos, 1983; Coyle & Reece, 1966) as shown in Figure 11. Frame element is chosen from the library of the SAP2000 to model the behaviour of a pile. The diameter of the pile is 1210 mm and penetrates into 80 m in the soil. In order to simulate the structure-pile–soil interaction through several layers of different soils, the piles are divided along their vertical axis such that within each layer of the soils the portion of the pile is divided into 1.0-m long segments. The relative movement between the pile and soil can be simplified into a number of non-linear vertical springs representing the vertical friction force exerted by the soil on the pile surface. For each pile, there is also an end support spring, which represents the end-bearing capacity of the pile. Figure 12 illustrates the arrangement of the vertical and end bearing soil springs. The spring parameters are calculated according to the site investigation and pile testing data (PTTEP International, 2010).

4. Validation of the proposed methodology

In order to validate the proposed LCC methodology, a comparison is made with the results obtained from a more rigorous method referred to as the 'reference method'. In the reference method, most of the simplifications made in this paper are avoided. The whole structure, i.e. the MDOF system, is used instead of the ESDOF system, and the full fragility and IDA curves are constructed instead of the approximated ones to capture accurately the dispersion in structural capacity as well as seismic demand. In addition, for each hazard, 20 records are used instead of 10 to represent accurately the dispersion in demand associated with each hazard level. The IDA curves of the FB-Conv and FB-BRB models for both the MDOF and the ESDOF systems are shown in Figures 13 and 14, respectively. Figure 15 shows a comparison between the mean IDA curves of the MDOF and the ESDOF systems for both FB-Conv and FB-BRB models. It can be observed that at relatively small spectral acceleration (.4 g for FB-Conv and .9 g for FB_BRB), the two results are almost identical. As the seismic intensity further increases there are slight differences between the two results; and the difference is larger in the structure with BRB than in the structure with conventional bracing. However, considering the similar overall shapes of the curves and the simplicity of the ESDOF systems, the results are satisfactory.
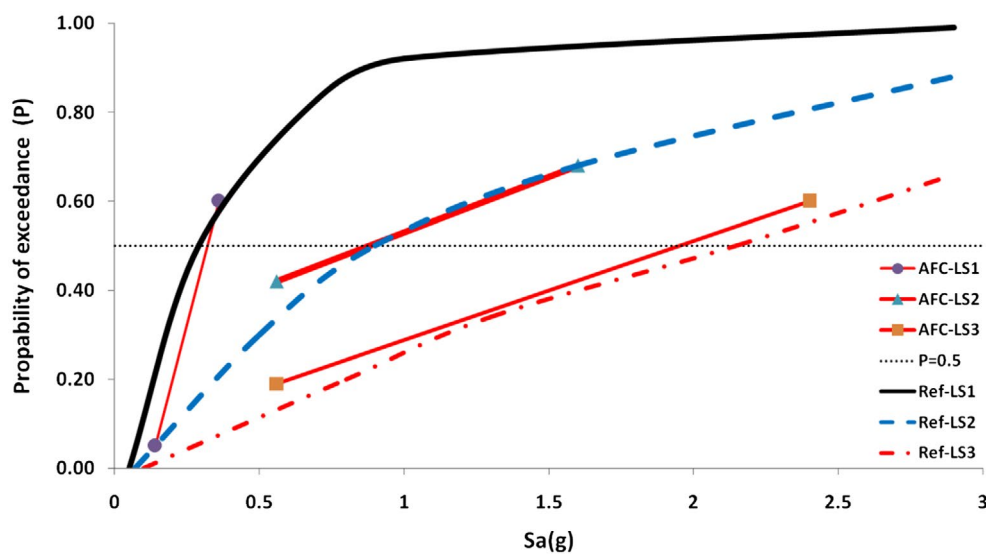
Figure 16 shows the Fragility curves of the FB-Conv model at each limit state obtained from the reference method (Ref) and the approximate method (AFC) with the difference in $S_a^{\hat{c}}$ indicated on the figure. As shown from the figures, the difference in $S_a^{\hat{c}}$ at $P(\mathrm{LS}_{|s_a}) = .5$ is marginal for LS1 and LS2 (.01 and .02 g, respectively). However, the difference is larger for the LS3 (.15 g). As

Table 5. S_a and corresponding P_i used for constructing the AFC for FB-Conv model.

Return period (years)	S_a(g)	P_i(LS1)	P_i(LS2)	P_i(LS3)
200	.14	.05	0	0
1000	.36	.6	.18	.06
2500	.56	.83	.42	.19
–	1.6*	–	.68	–
–	2.4*	–	–	.6

Notes: The shaded cells indicate the values used for constructing the AFC. Two points only are required for each limit state.
*These values are assumed using engineering judgement to obtain values of P_i more than .5.
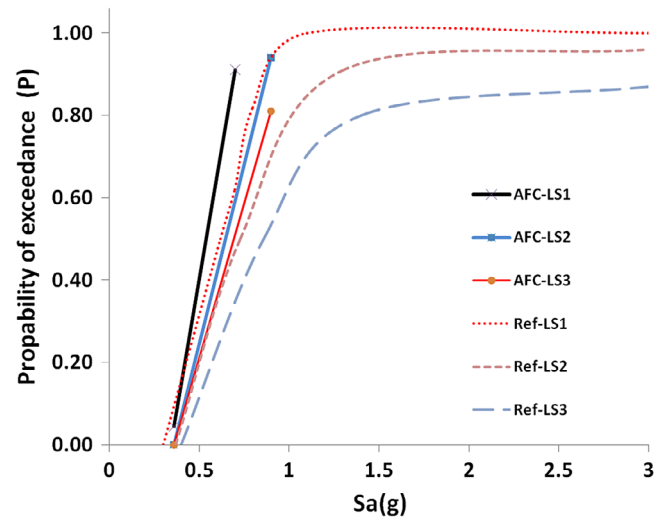
Figure 17. Fragility curves of the FB-BRB model at three limit states obtained from the reference method (Ref) and the approximate method (AFC).

Table 6. S_a and corresponding P_i used for constructing the AFC for FB-BRB model.

	S_a(g)	P_i(LS1)	P_i(LS2)	P_i(LS3)
200	.08	0	0	0
1000	.24	.025	0	0
2500	.36	.03	0	0
–	.7*	.88	–	–
–	.9*	–	.92	.77

Notes: The shaded cells indicate the values used for constructing the AFC. Two points only are required for each limit state.
*These values are assumed using engineering judgement to obtain values of P_i more than .5.

observed in Figure 15, the enhanced differences in LS3 limit state are contributed largely from the reduced accuracy of the ESDOF systems in comparison with the original models at higher seismic intensity level. Table 5 shows the points used for the construction of the AFC. The shaded cells in the table indicate the values used for constructing the AFC. Only two points are sufficient for each limit state to draw the strait portion of the AFC.

It is worth to mention that $P(\mathrm{LS}_{|s_a})$ calculated for the 200, 1000 and 2500 yr hazards are not enough to make a straight line crossing the $P(\mathrm{LS}_{|s_a}) = .5$ (as the case in LS2 and LS3), then engineering judgement should be made to decide appropriate spectral acceleration that results in $P(\mathrm{LS}_{|s_a})$ values that can be fitted across .5. As shown in Table 5, the S_a values required for LS2 and LS3 are 1.6 and 2.4 g, respectively. These values of S_a will result in $P(\mathrm{LS}_{|s_a})$ equal to .68 and .6, respectively. Figure 17

Table 7. Summary of the parameters used in LCC estimation for FB-Conv model.

Parameter Limit state	MDOF (reference)			ESDOF(proposed)			Note
	LS1	LS2	LS3	LS1	LS2	LS3	
MIDR, %	1	2	3	1	2	3	% of Jacket height
L, (years)		30			30		
$S_a^{\hat{c}}$, g	.28	.90	2.1	.29	.92	1.95	
$\beta_{D|s_a}$	.31	.07	.41	.32	.07	.51	
$H(S_a)$	.0065	.00050	.00008	.00602	.00048	.00009	
k_o		1.63E-04			1.48E-04		
k		1.88			1.80		
b		1.50			1.86		
β_C		.3			.3		
$P(LS_{|s_a})$, %	.75	.054	.01	.66	.050	.011	at $S_a^{\hat{c}}$
P_i, %	.70	.045	.01	.609	.039	.011	
V, m³		28.9			28.9		
C_o, $		28,900			28,900		Assuming 1000$/m³ of steel
C_i, $	8670	14,450	20,230	8670	14,450	20,230	Assuming .3, .5 and .7 of C_o, respectively
λ		.03			.03		
q		.029			.029		$= \ln(1+\lambda)$
α		.66			.66		$= 1 - \exp(-ql)/ql$
LCC, $		30,237			30,106		
$(LCC - C_o)$, $		1373			1206		Additional cost
$(D_{Ref} - D_{Proposed})/C_o$, %		−			.003		

Table 8. Summary of the parameters used in LCC estimation for FB-BRB model.

Parameter Limit state	MDOF (reference)			ESDOF(proposed)			Note
	LS1	LS2	LS3	LS1	LS2	LS3	
MIDR, %	1	2	3	1	2	3	% of Jacket height
L, (years)		30			30		
$S_a^{\hat{c}}$, g	.65	.70	.85	.55	.65	.70	
$\beta_{D|s_a}$	.47	.46	.38	.62	.59	.56	
$H(s_a)$	.00103	.00087	.00057	.00148	.00103	.00087	
k_o		8.28E-05			8.38E-05		
k		1.94			1.63		
b		.404			.544		
β_C		.3			.3		
$P(LS_{|s_a})$, %	1.51	1.19	.43	2.16	1.22	.85	at $S_a^{\hat{c}}$
P_i, %	.33	.75	.43	.94	.37	.84	
V, m³		20.8			20.8		
C_o, $		20,800			20,800		Assuming 1000$/1.0 m³ of steel
C_i, $	6240	10,400	14,560	6240	10,400	14,560	Assuming .3, .5 and .7 of C_o, respectively
λ		.03			.03		
q		.029			.029		$= \ln(1+\lambda)$
α		.66			.66		$= 1 - \exp(-ql)/ql$
LCC, $		27,433			25,190		
$D = (LCC - C_o)$, $		6632			4390		Additional cost
$(D_{Ref} - D_{Proposed})/C_o$, %		−			10.78		

presents the fragility curves of the FB-BRB model at three limit states obtained from the reference method (Ref) and the approximate method (AFC). As observed in the results of the FB-Conv model, the difference in $S_a^{\hat{c}}$, at $P(LS_{|s_a}) = .5$ increases from .1 g in the LS1 and LS2 limit states to .15 g in the LS3. Table 6 shows the points used for the construction of the AFC. The shaded cells in the table indicate the values used for constructing the AFC.

Results of the LCC estimation obtained using the proposed and the reference methods are compared in Tables 7 and 8 for FB-Conv and FB-BRB, respectively. According to the analysis results, the LCCs estimated by the proposed method are slightly (in case of FB-Conv) or marginally (in case of FB-BRB) different compared to those of the reference method. In the FB-Conv model, the LCCs obtained from the reference and the approximate methods are $ 30,237 and $ 30,106, respectively, which differ in about .4%. On the other hand, the LCCs obtained for the FB-BRB model are $ 27,433 and $ 25,190, respectively,

which differ in about 11%. In the FB-BRB case with relatively large discrepancy, the ESDOF system approximation seems to be insufficient to capture accurately the actual behaviour of the original structure, especially in the structural response with large deformation. This can be attributed primarily to the inaccurate representation of the nonlinear hysteretic behaviour of BRB in the ESDOF model, which plays a significant role in the structure response accompanied with large nonlinear deformation.

Another reason that should be highlighted in this context is that the radiation damping of the soil is considered only in the MDOF model used for the reference method, whereas it is implicitly included in the capacity curve of the ESDOF system but not considered explicitly during the detailed NLTHA. Another reason for the inaccuracy is the contribution of the soil–pile interaction to the global response of the super-structure of the platform, which is neglected in the ESDOF system. Those effects are more pronounced in high seismic hazards. Nevertheless, the

agreement between the proposed and the reference methods is generally adequate considering the assumptions under which the LCC is estimated. Recognising that there is a trade-off between maintaining the required accuracy and achieving simplicity, the proposed method seems to be an efficient tool for LCC evaluation of structures for practical use.

5. Conclusions

In this study, a simplified procedure for an LCC framework was proposed. This framework incorporated the details of hazard selection, limit state definition, damage probability calculation for each limit state and a formulation of the total LCC. The methodology is advantageous compared to conventional methods in terms of simple inclusion of the demand and capacity uncertainties. The proposed methodology was validated by applying it to a fixed-type steel offshore platform structure composed of hollow steel sections located in Gulf of Moattama, offshore Myanmar. In order to investigate the effect of using different bracing systems on the seismic LCC of the offshore platform, the seismic performances of the model structures with BRB were investigated in comparison with those of the structure with conventional bracing.

According to the analysis results, the LCCs estimated by the proposed method were somewhat different compared to those obtained from a more rigorous method. The maximum difference was in the order of 10.8% in the structure designed with buckling-restrained bracing, and was almost negligible for the FB-Conv case. The discrepancy in the LCC estimation came, primarily, from the use of the equivalent single degree of system, AFCs and the LIDA curves. Based on the analysis results, it was concluded that the method might be recommended as a convenient tool for LCC estimation and optimum design of fixed type offshore platform structures.

Disclosure statement

No potential conflict of interest was reported by the authors.

Funding

References

Abdel Raheem, S. E. (2013). Nonlinear response of fixed jacket offshore platform under structural and wave loads. *Coupled Systems Mechanics, 2*, 111–126.

AISC.ANSI/AISC 360-05. (2005). *Specifications for structural steel buildings*. Chicago, IL: American Institute of Steel Construction.

Anagnostopoulos, S. A. (1983). Pile foundation modelling for inelastic earthquake analyses of large structures. *Engineering Structures, 5*, 215–222.

Ang, A. H.-S., & Leon, D. D. (1997). Determination of optimal target reliabilities for design and upgrading of structures. *Structural Safety, 19*, 91–103.

Ang, A. H. S., & Lee, J. C. (2001). Cost optimal design of R/C buildings. *Reliability Engineering and System Safety, 73*, 233–238.

API RP-2A. (2000). *American petroleum institute recommended practice for planning, design and constructing fixed offshore platforms* (21st ed.). Washington: Author.

Aslani, H. (2005). *Probabilistic earthquake loss estimation and loss disaggregation in buildings* (PhD Thesis). John A. Blume Earthquake Engineering Centre, Department of Civil and Environmental Engineering Stanford University, Stanford, CA, USA.

Aslani, H., & Miranda, E. (2005). Probability-based seismic response analysis. *Engineering Structures, 27*, 1151–1163.

Bea, R. G., Brandtzaeg, A., & Craig, M. J. K. (1998). Life-cycle reliability characteristics of minimum structures. *ASME Journal of Offshore Mechanics and Arctic Engineering, 120*, 129–138.

Cornell, C. A., Jalayer, F., Hamburger, R. O., & Foutch, D. A. (2002). Probabilistic basis for 2000 SAC Federal Emergency Management Agency steel moment frame guidelines. *ASCE Journal of Structural Engineering, 128*, 526–533.

Coyle, H. M., & Reece, L. C. (1966). Load transfer for axially loaded piles in clay. *ASCE Journal of the Soil Mechanics and Foundations Division, 92*(2), 1–26.

De Leon, D., & Ang, A. H.-S. (2002). Development of a cost-benefit model for the management of structural risk on oil facilities in Mexico. *Computational Structural Engineering, 2*, 19–23.

Dolsek, M. (2012). Simplified method for seismic risk assessment of buildings with consideration of aleatory and epistemic uncertainty. *Structure and Infrastructure Engineering, 8*, 939–953.

Ellingwood, B. R., & Wen, Y. K. (2005). Risk-benefit-based design decisions for low probability/high consequence earthquake events in Mid-America. *Progress in Structural Engineering Materials, 7*, 56–70.

Fajfar, P. (2002). *Structural analysis in earthquake engineering – A breakthrough of simplified non-linear methods*. Proceedings of 12th European conference on earthquake engineering, London, UK, Paper No. 843.

FEMA P58-1. (2012). *Seismic performance assessment of buildings: 1 – Methodology*. Prepared by the Applied Technology Council for the Federal Emergency Management Agency, Washington, DC, USA.

FEMA P695. (2009). *Quantification of building seismic performance factors*. Prepared by the Applied Technology Council for the Federal Emergency Management Agency, Washington, DC, USA.

FEMA P-750. (2009). *NEHRP recommended seismic provisions for new buildings and other structures*. Washington, DC: Building Seismic Safety Council.

FEMA 356. (2000). *Pre-standard and commentary for the seismic rehabilitation of buildings*. Prepared by the American Society of Civil Engineers for the Federal Emergency Management Agency, Washington, DC, USA.

Fragiadakis, M., & Vamvatsikos, D. (2010). Fast performance uncertainty estimation via pushover and approximate IDA. *Earthquake Engineering and Structural Dynamics, 39*, 683–703.

Fragiadakis, M., Lagaros, N. D., & Papadrakakis, M. (2006). Performance-based multi objective optimum design of steel structures considering life-cycle cost. *Structural & Multidisciplinary Optimization, 32*(1), 1–11.

Garbatov, Y., & Soares, C. G. (2001). Cost and reliability based strategies for fatigue maintenance planning of floating structures. *Reliability Engineering & System Safety, 73*, 293–301.

Gencturk, B. (2013). Life-cycle cost assessment of RC and ECC frames using structural optimization. *Earthquake Engineering and Structural Dynamics, 42*, 61–79.

Goda, K., Lee, C. S., & Hong, H. P. (2010). Lifecycle cost–benefit analysis of isolated buildings. *Structural Safety, 32*, 52–63.

Golafshani, A. A., Tabeshpour, M. R., & Komachi, Y. (2009). FEMA approaches in seismic assessment of jacket platforms (case study: Ressalat jacket of Persian gulf). *Journal of Constructional Steel Research, 65*, 1979–1986.

Hancock, J., Bommer, J. J., & Stafford, P. (2008). Numbers of scaled and matched accelerograms required for inelastic dynamic analyses. *Earthquake Engineering and Structural Dynamics, 37*, 1585–1607.

Hancock, J., Watson-Lamprey, J., Abrahamson, N. A., Bommer, J. J., Markatis, A., McCoy, E., & Mendis, R. (2006). An improved method of matching response spectra of recorded earthquake ground-motion using wavelets. *Journal of Earthquake Engineering, 10*, 67–89.

Hiraishi, H., Midorikawa, M., Teshigawara, M., & Gojo, W. (1998). *Development of performance-based building code in Japan – Framework of seismic and structural provisions*. 2nd U.S.-Japan Workshop on Performance-Based Engineering, Applied Technology Council (ATC), San Francisco, CA, USA.

Iervolino, I., & Cornell, C.A. (2005). Record selection for nonlinear seismic analysis of structures. *Earthquake Spectra, 21*, 685–713.

Jeong, S. H., & Elnashai, A. S. (2007). Probabilistic fragility analysis parameterized by fundamental response quantities. *Engineering Structures, 29*, 1238–1251.

Kramer, S. L. (1996). *Geotechnical earthquake engineering* (1st ed.). Upple Saddle River, NJ: Prentice Hall.

Li, G., Zhang, D., & Yue, Q. (2009). Life-cycle cost-effective optimum design of ice-resistant offshore platforms. *ASME Journal of Offshore Mechanics and Arctic Engineering, 131*, 031501-031501-9.

Luco, N., & Cornell, C. A. (2001). Structure-specific scalar intensity measures for near-source and ordinary earthquake ground motions. *Earthquake Spectra, 23*, 357–392.

Luco, N., & Bazzurro, P. (2007). Does amplitude scaling of ground motion records result in biased nonlinear structural drift responses? *Earthquake Engineering and Structural Dynamics, 36*, 1813–1835.

Matlock, H. (1970). *Correlations for design of laterally loaded piles in soft clay*. Proceedings of offshore technology conference, Richardson, Houston, TX, USA, pp. 577–594.

Nour El-Din, M., & Kim, J. K. (2015). Seismic performance of pile-founded fixed jacket platforms with chevron braces. *Structure and Infrastructure Engineering, 11*, 776–795.

Pacific Earthquake Engineering Research (PEER) Center. (2013). *Strong motion database*. Berkeley, CA. Retrieved from http://ngawest2.berkeley.edu/

Pinna, R., Ronalds, B. F., & Andrich, M. A. (2003). Cost-effective design criteria for australian monopod platforms. *ASME Journal of Offshore Mechanic and Artic Engineering, 125*, 132–138.

Pinto, P. E., Giannini, R., & Franchin, P. (2004). *Seismic reliability analysis of structures*. Pavia: *IUSS Press*.

PTTEP International. (2010). *Provision of earthquake specific engineering services (site study) for Myanmar Engineering Zawtika Project, Geotechnical Earthquake Engineering Addendum, Doc. No. 09-214-H4*.

Qi, X., & Moehle, J. P. (1991). *Displacement design approach for reinforced concrete structures subjected to earthquakes*. Berkeley, CA: Earthquake Engineering Research Center.

SAP2000. (2005). *Structural analysis program, version 10 analysis reference manual*. Berkeley, CA: Computers and Structures Inc.

Shome, N., Cornell, C. A., Bazzurro, P., & Carballo, J. E. (1998). Earthquakes, records, and nonlinear responses. *Earthquake Spectra, 14*, 469–500.

Sullivan, T. J., Welch, D. P., & Calvi, G. M. (2014). Simplified seismic performance assessment and implications for seismic design. *Earthquake Engineering and Engineering Vibrations, 13*, 95–122.

Taflanidis, A. A., & Beck, J. L. (2009). Life-cycle cost optimal design of passive dissipative devices. *Structural Safety, 31*, 508–522.

Val, D. V., & Stewart, M. G. (2003). Life-cycle cost analysis of reinforced concrete structures in marine environments. *Structural Safety, 25*, 343–362.

Welch, D. P., Sullivan, T. J., & Calvi, G. M. (2014). Developing direct displacement-based procedures for simplified loss assessment in performance-based earthquake engineering. *Journal of Earthquake Engineering., 18*, 290–322.

Wen, Y. K., & Foutch, D. A. (1997). *Proposed statistical and reliability framework for comparing and evaluating predictive models for evaluation, design, and critical issues in developing such framework*. SAC/BD-97/03, SAC Joint Venture, USA.

Wen, Y. K. & Kang, Y. J. (2001). Minimum building life-cycle cost design criteria. i: methodology. *ASCE Journal of Structural Engineering, 127*, 330–337.

Yun, S. Y., & Foutch, D. A. (2000). *Performance prediction and evaluation of low ductility steel moment frames for seismic loads*. SAC Background Rep. No. SAC/BD-00/26, SAC Joint Venture, Richmond, California, USA.

Zhang, D. Y., Li, G., & Yue, Q. J. (2005). State of the art of structural optimization for offshore platforms. *Ocean Engineering, 23*, 107–112.